Smart Materials in Medicine 5 (2024) 281–290

Contents lists available at ScienceDirect

Smart Materials in Medicine

journal homepage: www.keaipublishing.com/en/journals/smart-materials-in-medicine/

Hydrogel-fiber-mesh-based 3D cell cultures: A new method for studying pituitary tumors

Wooju Jeong [a,1], Sungrok Wang [b,1], Yumin Kim [a], Soohyun Lee [c], Minhu Huang [b], Jaeil Park [b], Myung-Han Yoon [b,**], Chang-Myung Oh [a,*], Cheol Ryong Ku [c,***]

[a] Department of Biomedical Science and Engineering, Gwangju Institute of Science and Technology, Gwangju, South Korea
[b] School of Materials Science and Engineering, Gwangju Institute of Science and Technology, Gwangju, South Korea
[c] Department of Internal Medicine, Severance Hospital, Yonsei University College of Medicine, Seoul, South Korea

ARTICLE INFO

Keywords:
Pituitary tumor
Acromegaly
Hydrogel-fiber meshes
3D cell culture
GH3 cells

ABSTRACT

Acromegaly is a challenging medical condition that arises from the excessive production of growth hormones and the insulin-like growth factor 1 in the pituitary gland. While surgery is the primary treatment for acromegaly, medication is increasingly being used in patients who are unsuitable for surgery or have experienced treatment failure. Despite advancements in medical and surgical therapies, the treatment of acromegaly remains challenging. In this research, a three-dimensional (3D) *in-vitro* cell culture model for pituitary adenoma research was developed using hydrogel fiber meshes (HFMs) and GH3 cells. Electrospun nanofibers based on polyvinyl alcohol and polyacrylic acid were converted into HFMs by hydrogelification with the leaching of electrosprayed cellulose acetate beads for porosity enhancement. GH3 cells grown in the 3D model exhibited increased dispersion and upregulation of the somatostatin receptor subtypes 2 and 5 compared to those grown in traditional 2D cultures, as well as high sensitivity to somatostatin analogs and tumor-like profiles (as indicated by functional assays and transcriptome analysis, respectively). Therefore, the proposed 3D model accurately represents the physiological response to pituitary-adenoma therapeutic agents. This study highlights the potential of HFMs as a versatile platform for 3D *in-vitro* cell culture models that can be employed for pituitary adenoma research. Moreover, the proposed 3D cell culture model may contribute to a deeper understanding of tumor biology and facilitate the development of effective therapeutic strategies for acromegaly.

1. Introduction

Acromegaly is a medical condition that occurs due to the overproduction of the growth hormone (GH) and insulin-like growth factor 1 (IGF-1) by pituitary GH-secreting adenoma [1]. Excessive GH secretion leads to a range of physical and metabolic complications including cardiovascular disease, diabetes, and malignancies, which significantly influence the overall human health [2,3]. Untreated acromegaly can significantly increase the risk of mortality [4]. The first-line treatment for acromegaly involves the transsphenoidal/ethmoidal surgical resection of the pituitary adenoma followed by adjunctive radiotherapy and/or pharmacological intervention, to ensure the adequate control of GH and IGF-1 levels [4]. Despite recent advances in the medical and surgical treatment of patients with acromegaly, their management remains associated with significant challenges. Permanent cure or sustained biochemical control after surgical intervention is not observed in a substantial proportion of patients (less than 65% of patients exhibit optimal results); furthermore, the success rate decreases to ~45% in patients treated with the first-generation somatostatin receptor ligands (SRLs) [5].

The treatment and management of treatment-resistant acromegaly is extremely challenging. The absence of an appropriate drug-screening model significantly limits the treatment of patients with drug-resistant acromegaly. The GH3 somatotropic cell line (GH3 cells) that is derived from the pituitary tumor of a female rat has been widely used for *in-vitro*

* Corresponding author. Department of Biomedical Science & Engineering, Gwangju Institute of Science and Technology, Gwangju, 61005, South Korea.
** Corresponding author. School of Materials Science and Engineering, Gwangju Institute of Science and Technology, Gwangju, 61005, South Korea.
*** Corresponding author. Endocrinology, Institute of Endocrine Research, Department of Internal Medicine, Severance Hospital Pituitary Tumor Center, Yonsei University College of Medicine, 50-1 Yonsei-ro, Seodaemun-gu, Seoul, 03722, South Korea.
E-mail addresses: mhyoon@gist.ac.kr (M.-H. Yoon), cmoh@gist.ac.kr (C.-M. Oh), CR079@yuhs.ac (C.R. Ku).
[1] These authors contributed equally to this paper.

https://doi.org/10.1016/j.smaim.2024.03.004
Received 14 November 2023; Received in revised form 7 March 2024; Accepted 9 March 2024

Abbreviations

PVA	polyvinyl alcohol
PAA	polyacrylic acid
CA	cellulose acetate
OCT	octreotide acetate
PAS	pasireotide
SSTR	somatostatin receptor
PDL:	poly-D-lysine
SEM	scanning electron microscopy
TEM	transmission electron microscopy
GH	growth hormone
NFM	crosslinked electrospun fiber mesh
HFM	hydrogel fiber mesh

studies of the somatostatin system and GH secretion [6,7]. However, the investigation of pituitary disease with this cell line is associated with several limitations [8,9]. First, similar to the *SH-SY5Y* neuroblastoma cell line, GH3 cells comprise loosely adherent cells with clusters of freely floating cells [7,10,11]. As both the adherent and floating GH cells are viable, it is vital to consider the characteristics and drug responses of both cell types during *in-vitro* assays. Second, GH3 cells exhibit a low response to somatostatin analogs (i.e., drugs that are widely used for acromegaly treatment). Octreotide acetate (OCT) and pasireotide (PAS) are common somatostatin analogs; neither OCT nor PAS significantly reduces GH secretion in GH3 cells after 24 h of exposure. Moreover, these drugs are ineffective in suppressing GH3 cell-induced angiogenesis as observed in an *in vitro* zebrafish embryo model [7].

Recent studies indicate that three-dimensional (3D) cell culture methods exhibit superior performance compared with traditional two-dimensional (2D) cell culture methods [12–14]. As shown in Fig. 1a and b, 3D cell cultures can be used to create organ-like structures with microenvironments that accurately emulate the physiology of target organs [15,16] or provide mechanical cues for cell behavior regulation [17–20]. Moreover, this novel technique exhibits high potential for the development of *in-vitro* models that closely mimic pituitary tumor physiology for drug screening applications [21,22]. Zhang et al. attempted to develop a pituitary tumoroid model from human pituitary corticotroph tumor cells using a two-step culture system based on 3D Matrigel culture and subsequent expansion in a spinner flask [21]. Although their paper reports the maintenance of adrenocorticotropic hormone (ACTH) secretion in a corticotroph-tumor model for more than two passages, it does not contain functional studies on growth hormone regulation [21]. Similarly, Krokker et al. proposed a 3D cell culture model based on RC-4B/C and GH3 cells for somatotrophic tumors. Although they engineered a 3D culture model comprising spheroids (cultivated using spheroid-inducing media within Matrigel), they did not use the proposed pituitary-tumor model for hormonal studies [22]. Additionally, both the aforementioned models are based on Matrigel, which exhibits considerable inter-batch variability and lacks physical and biochemical controllability. These factors hinder the fine tuning of the extracellular matrix (ECM) (which promotes specific cellular behavior with targeted biological outcomes), making the models unsuitable for imaging studies [23].

Therefore, it is vital to develop new 3D cell culture models as a reliable platform for studying pituitary somatotroph cells. This is particularly pertinent in emulating the ECM of pituitary adenomas, which predominantly comprise type I and type III collagen [24,25], characterized by their fibrous structure. This insight corresponds to advances in tissue engineering, where fibrous scaffolds are increasingly recognized owing to their ability to mimic *in vivo*-like environments and facilitated interactions with cells. In contrast to flat bulk hydrogels, the diverse impacts of fibrous scaffolds are primarily attributed to mechanosensing and directional guidance for cellular growth along the fibers [26]. Consequently, cells on fibrous scaffolds typically demonstrate uniaxial growth, and their migration rate and/or spread area vary depending on the modulus of individual fibers. Moreover, as cells can exert forces on individual fibers, the dynamic interplay between cells and fibers gives rise to unique behaviors, for instance, slingshot migration of cells with stretching and recoiling of fibers or recruitment of fibers by contraction of adherent cells, which are not typically observed in conventional bulk hydrogels used in 3D cell cultures [27,28]. From this perspective, in principle, it is possible to develop 3D-culture pituitary somatotroph models using GH3 cells and electrospun nanofibrous meshes. Typical electrospun polymer nanofibers, however, exhibit optical scattering that impedes clear microscopic imaging, mechanical stiffness that is unfavorable for cell culture, and limited cell infiltration owing to small pores [29]. Therefore, several strategies have been proposed to overcome the abovementioned issues related electrospun nanofiber meshes (NFMs), particularly, to increase porosity in solid nanofiber scaffolds. According to a report by Benjamin et al., femtosecond-laser ablation produced uniform pores on electrospun fiber meshes by promoting cell infiltration [30]. A paper by Mahesh et al. demonstrated the construction of macroporous NFMs by a gas-foaming technique [31]. Ice-crystal templating during the electrospinning of hydrophobic polymers, a technique labeled cryogenic electrospinning, was also used to produce highly porous polymer meshes [32–34]. Nonetheless, there exist very few reports on nanofiber-based scaffolds with not only large porosity but also mechanical softness and optical transparency so that they can effectively emulate realistic biological tissue environments.

In this study, highly porous hydrogel fiber meshes (HFMs) based on polyvinyl alcohol (PVA) and polyacrylic acid (PAA) were developed. Subsequently, their applicability as 3D cell culture models for pituitary adenoma research was investigated using GH3 cells. Previous studies report the utilization of specialized equipment to enhance the porosity of electrospun nanofiber meshes. On the contrary, in this study, cellulose acetate (CA) microbeads were incorporated into electrospun PVA/PAA nanofibers by the concurrent electrospraying to impede the stacking of nanofibers. Electrospun PVA/PAA nanofibers were converted into HFMs by PVA-PAA thermal crosslinking, followed by concentrated sulfuric acid (c-H_2SO_4) treatment (*hydrogelification*) [35,36] followed by the selective leaching of electrosprayed CA microbeads. This procedure generated highly porous HFMs with a large surface area for cell adhesion and growth in order to mimic native ECMs. Notably, PVA are partially sulfated during the concentrated sulfuric acid treatment, which is known as favorable for cell adhesion [37]. Therefore, the porous HFMs can also serve as a bioactive fibrous scaffold, while the high porosity of the HFMs can facilitate the effective mass transfer of essential nutrients, oxygen, and other soluble biological factors that are crucial for cell survival and function. In this study, the physiological characteristics of the proposed 3D cell culture scaffold and cellular responses to somatostatin analogs were investigated. Furthermore, the molecular signature of the new 3D cell culture model was analyzed by comparing the transcriptomes of GH3 cells cultured in 3D and 2D environments. Comprehensive analysis enables an in-depth understanding of the cellular and molecular mechanisms underlying the functions of the proposed HFM-based 3D cell culture model.

2. Results

2.1. Fabrication of porous HFMs for 3D cell culture

The growth pattern of GH3 cells in 2D cell cultures (in flat Petri dishes) indicates two distinct modes of cell growth that form adherent cells (Fig. S1a) and floating clusters (Fig. S1b) which is consistent with the previous literature[18]. Fig. 1b and c shows how HFMs are prepared in this study which was used as 3D cell cultures for GH3 cells. The HFMs were fabricated by the thermal annealing of electrospun PVA/PAA NFMs with electrosprayed CA microbeads (d ~11.3 μm) for crosslinking

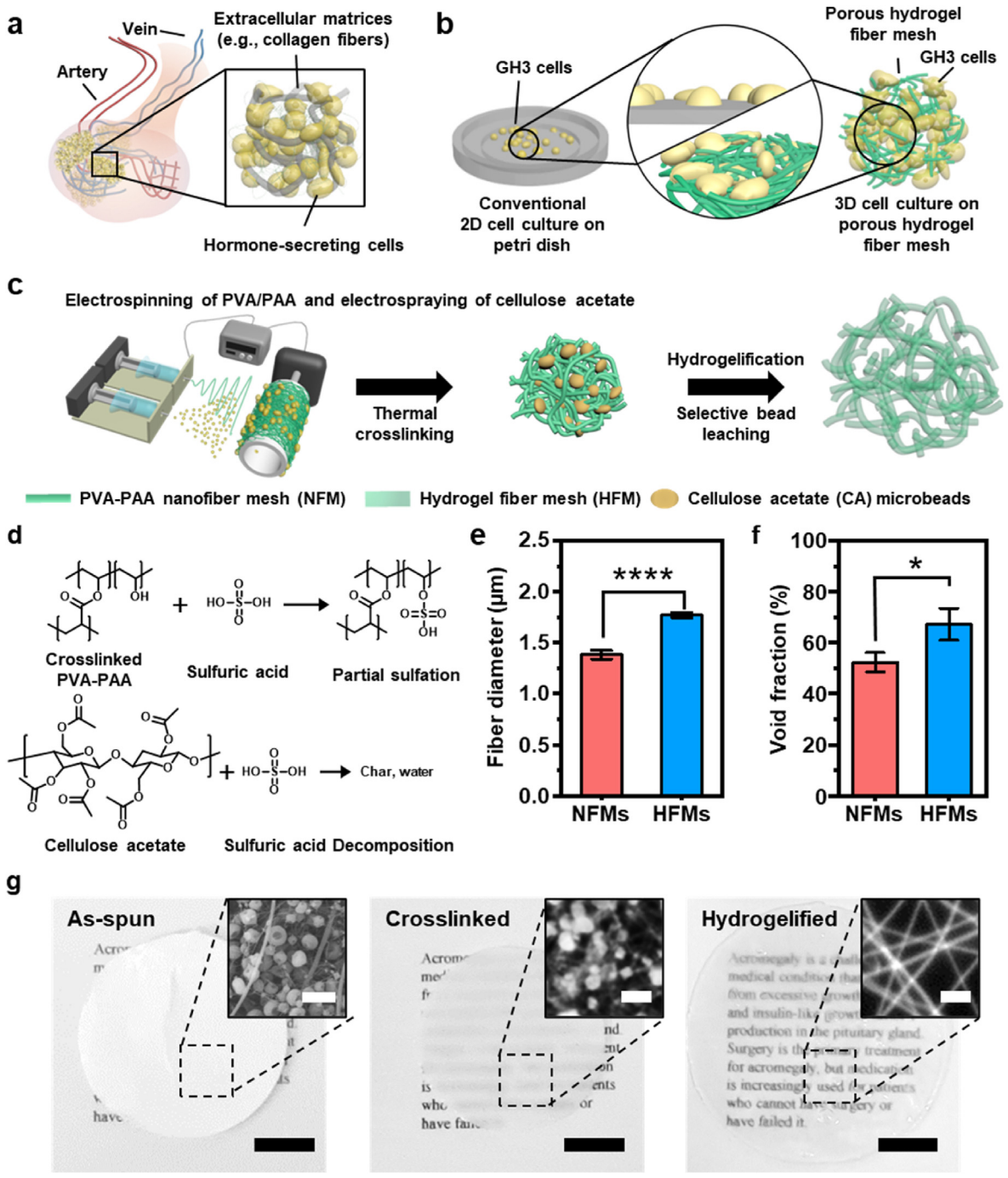

Fig. 1. Synthesis and characterization of porous hydrogel fiber meshes (HFMs) that mimic the pituitary gland.
Schematic illustrations of (a) the pituitary gland, (b) a conventional 2D-culture model based on a flat tissue-culture plate, and (c) a 3D-culture model based on a highly porous HFM containing GH3 cells that mimics hormone-secreting tissue. (c) Fabrication procedure for the HFM. First, PVA/PAA nanofibers are electrospun and CA microbeads are electrosprayed. Next, thermal annealing is used for chemical crosslinking. Finally, concentrated sulfuric acid (H_2SO_4) is used for hydrogelification and CA leaching. (d) Proposed mechanisms for the sulfation of cross-linked PVA/PAA and decomposition of CA on concentrated H_2SO_4 treatment. Plots of the (e) average fiber diameters and (f) void fractions of the nanofiber mesh (NFM; before H_2SO_4 treatment) and HFM (after H_2SO_4 treatment). For statistical validation, a two-tailed unpaired Student's t-test is used. *$P < 0.05$ and ****$P < 0.0001$. (g) Photographs of the electrospun PVA/PAA nanofibers and electrosprayed CA microbeads: (i) as-prepared, (ii) after immersion in water, and (iii) after hydrogelification. The insets show (i) the SEM image of dry sample and (ii), (iii) laser scanning confocal microscopy images of wet samples. Scale bars denote 1 cm (black) and 5 μm (white). Each error bar represents the mean standard deviation.

followed by treatment with concentrated sulfuric acid. Fig. 1c and d shows that the cross-linked PVA/PAA nanofibers remained stable under concentrated H_2SO_4 treatment, whereas, the CA microbeads were leached out by forming highly porous and swollen HFMs with sulfate groups [36,38]. As shown in Fig. 1e, the average fiber diameter of the HFM (1.77 μm) was larger than that of the NFM (1.38 μm) owing to the water-absorption capacity of sulfate groups in the former. Furthermore, the HFM shows a larger void fraction (i.e., higher porosity) than the NFM which did not undergo concentrated H_2SO_4 treatment. This is because the interfiber spacing in the former was enlarged by CA-microbead leaching (Fig. 1f). Fig. 1g shows photographs of the bulk electrospun PVA/PAA NFMs with CA microbeads before and after hydrogelification

(HG). In these images, the NFM with CA microbeads appears white and opaque; individual fibers and microbeads are distinguishable in the corresponding scanning electron microscopy (SEM) image (Fig. 1g (i) and inset). After immersion into water, the NFM with CA microbeads appears translucent, possibly, because the CA microbeads are hydrophobic (Fig. 1g (ii)); additionally, individual fibers and microbeads remain discernible, as confirmed by laser scanning confocal microscopy (Fig. 1g (ii) inset). After dipping into concentrated H_2SO_4 and water rinsing (i.e., hydrogelification), the PVA/PAA nanofibers transformed into a hydrogel with no CA microbeads by forming a transparent and enlarged HFM sheet (Fig. 1g (iii) and inset).

To modulate the HFM porosity, three types of HFM samples were fabricated by varying the concentration of the PVA/PAA precursor solution used for electrospinning and the inclusion of CA microbeads (average diameter: 1.73 μm). For analysis, HFM samples with small and large average fiber diameters (with average swollen-fiber diameters of 1.07 and 1.77 μm, respectively) were fabricated. The three synthesized HFM samples were labeled the following (according to the relative concentration of PVA/PAA and presence/absence of CA): (i) V-A-8-2 (small PVA/PAA nanofibers without CA microbeads), (ii) V-A-12-3 (large PVA/PAA nanofibers without CA microbeads), and (iii) V-A-12-3-CA (large PVA/PAA nanofibers with CA microbeads). Figs. S2a–c show SEM images of these samples before hydrogelification and laser confocal microscopy images after hydrogelification with diameter comparisons. Among all the samples analyzed, V-A-12-3-CA exhibited the largest void fraction (>60%) (Fig. S2d). Moreover, the concentration of H_2SO_4 significantly affects CA-microbead removal and PVA/PAA-nanofiber hydrogelification in V-A-12-3-CA. As shown in Fig. S3a, the removal of CA microbeads did not occur on treatment with low-concentration (0–25 v/v%) H_2SO_4, whereas, the treatment with high-concentration (>50 v/v %) H_2SO_4 caused the efficient removal of CA microbeads. Additionally, the average fiber diameter was increased slightly after the H_2SO_4 (75 v/v

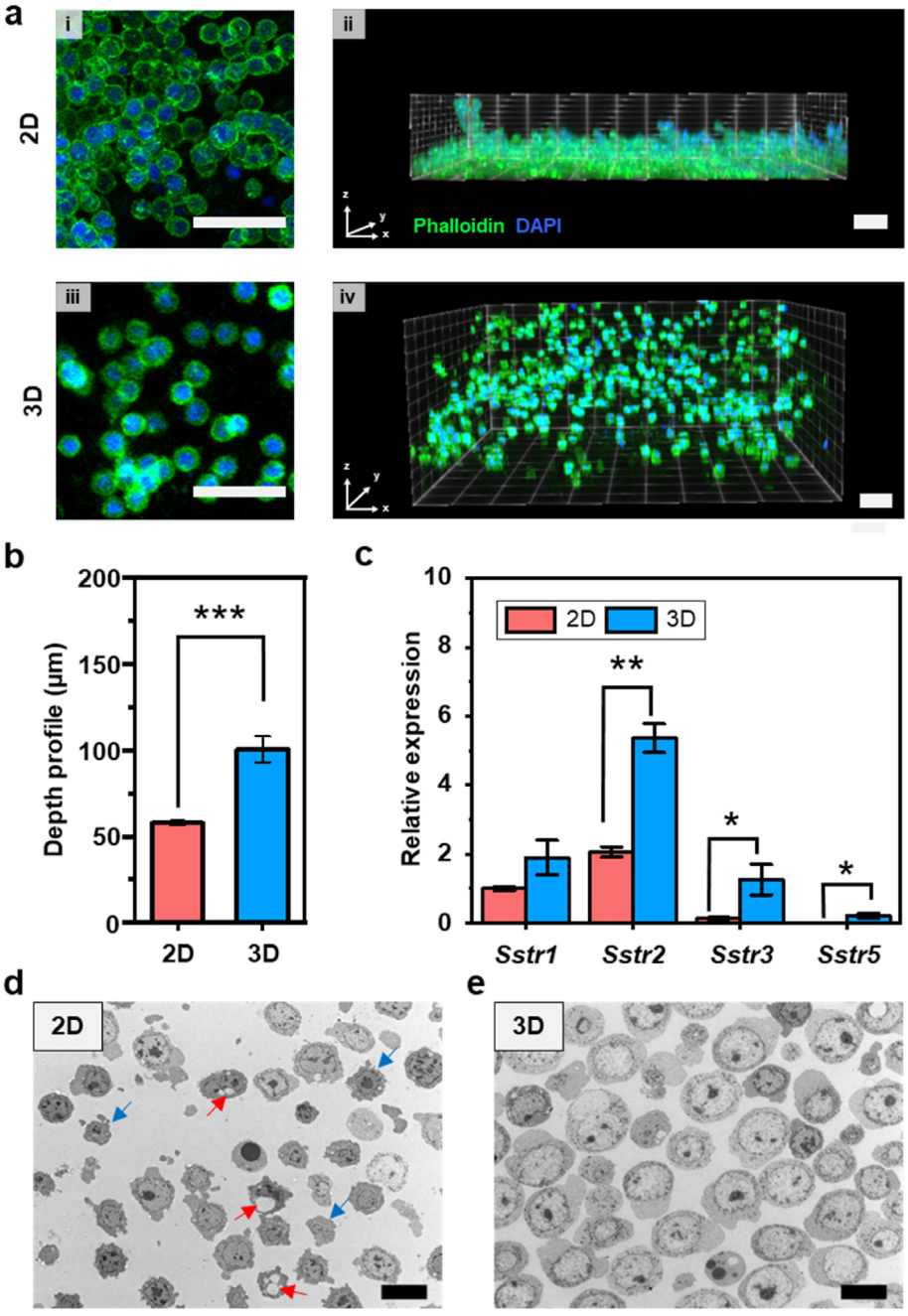

Fig. 2. GH3 cell behaviors in different culture systems.
(a) Confocal microscope images of fluorescence-stained GH3 cells under two different cell-culture conditions: conventional 2D cell culture on PDL-coated glass, and 3D cell culture on porous hydrogel fiber meshes. Images i and ii represent Z-projected and Z-stack images of the 2D culture, respectively, while images iii and iv display Z-projected and Z-stack images of the 3D culture, respectively. Green color indicates phalloidin (actin) and blue color indicates DAPI (nuclei). Scale bars correspond to 50 μm (b) Comparison of the depth profiles (i.e., penetration depth of cells). and (c) Relative expression of somatostatin receptors (SSTR 1, 2, 3, and 5) in 2D and 3D cultures. For statistical validation, a two-tailed unpaired Student's t-test is used. *P < 0.05, **P < 0.01, and ***P < 0.001. (d) Transmission electron microscopy (TEM) images of cells cultured in the 2D environment. (e) TEM images of cells cultured in the 3D environment. Red and blue arrows indicate autophagic bodies with intracellular vacuoles and apoptotic cells with irregular plasma membranes, respectively. Scale bars denote 10 μm.

%) treatment, but the average fiber diameter increased remarkably after the concentrated-H_2SO_4 (~100 v/v%) treatment.

2.2. Development of 3D in-vitro cell culture models for pituitary adenoma research

For 2D cell culture, GH3 cells were seeded on adherent flat dishes. To mitigate the formation of floating clusters, a poly-D-lysine (PDL) coating was applied to Petri dishes, as described in the previous literature [23]. PDL coating significantly reduced the number of cells floating in Petri dishes (Fig. S1c). For 3D culture, the cells were seeded into the fabricated HFMs without any coating. Interestingly, the HFM system contained a low number of floating cells, similar to the PDL-coated Petri dish. Representative confocal microscopy images of GH3 cells grown under both conditions are shown in Fig. 2a. GH3 cells in the HFMs exhibit more spatially dispersed growth (Fig. 2a (iii) and (iv)) than those in the PDL-coated Petri dishes (Fig. 2a (i) and (ii)). Notably, the cultured cells did not develop into tumor structures in the HFMs. Fig. 2b shows the depth profiles of the two systems, which indicates the average distance between the top and bottom cells; the GH3 cells cultured within the HFMs exhibit a significantly larger depth profile than those cultured on PDL-coated Petri dishes. In addition, we cultured GH3 cells in Matrigel which is one of the conventional 3D cell culture scaffolds for further comparison. The GH3 cells in Matrigel tend to grow in aggregates despite the bioactivity of Matrigel while those in HFMs exhibit evenly-dispersed morphologies due to the high porosity of the HFM scaffold and, possibly, the favorable cell-to-fiber (scaffold) interactions (Fig. S4).

This study indicates a significant alteration in the gene-expression profile of the somatostatin receptors (SSTRs) in GH3 cells cultured in a 3D environment compared to those cultured in traditional 2D

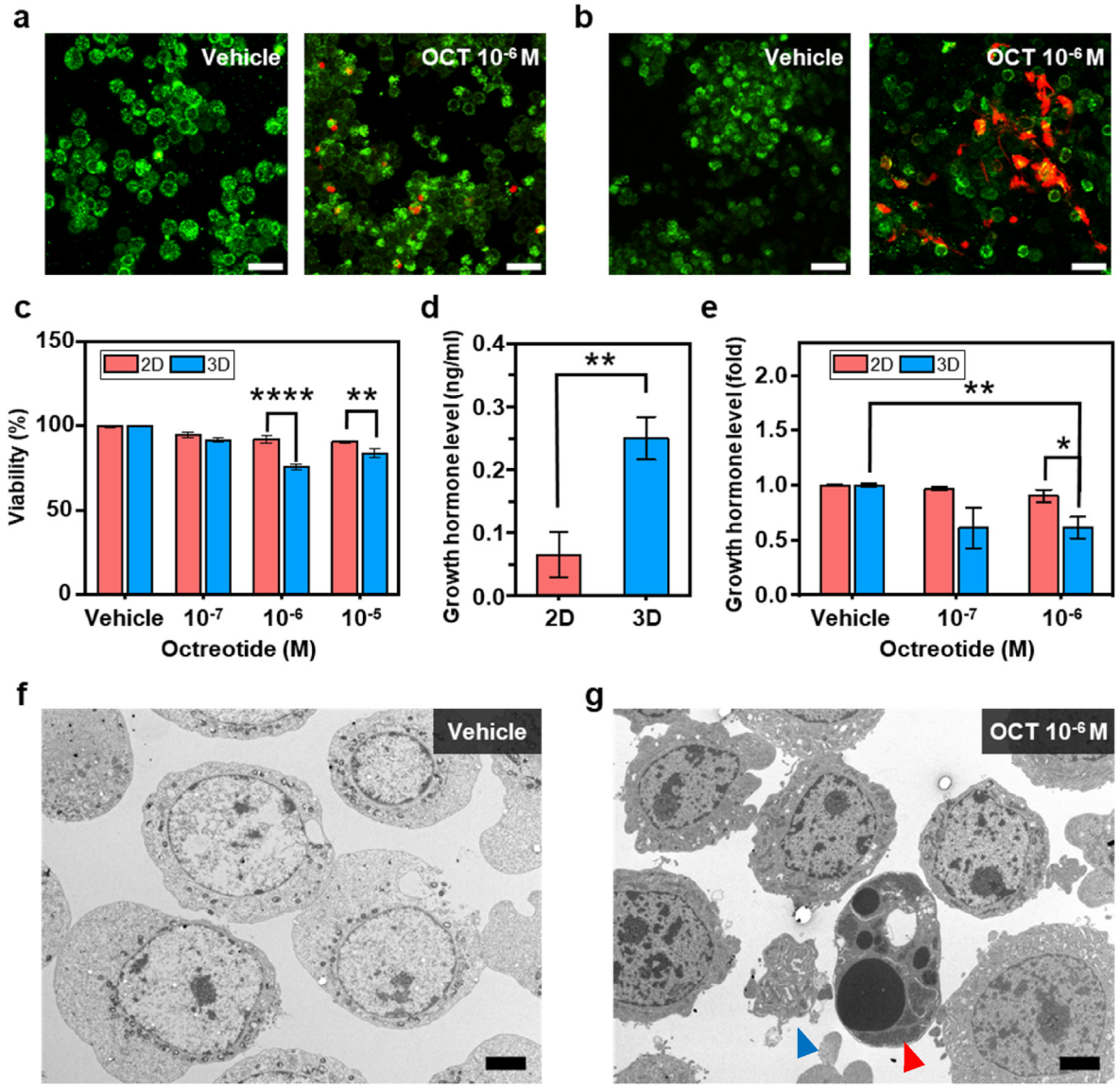

Fig. 3. Evaluation of the hormone-secreting function of GH3 cells in different culture systems.
cells after live and dead staining, treated with the vehicle (0.9% of saline solution) and 10^{-6} M of octreotide (OCT). Living cells are shown in green (stained by calcein AM) and dead cells are shown in red (stained by ethidium homodimer-1). Scale bars denote 50 μm. (c) Viability of GH3 cells treated with different concentrations of OCT in the 2D and 3D cell-culture systems. ELISA results for the growth hormone (GH) levels in media collected from the 2D- and 3D-cultured GH3 cells after (d) 1 h and (e) 3 h (with the vehicle and different concentrations of OCT). Figure (d) indicates significantly higher GH levels in the 3D-cultured cells than in the 2D-cultured cells. Figure (e) indicates a significant decrease in GH levels in the 3D-cultured cells after OCT (10^{-6} M) treatment. Representative TEM images of 3D-cultured GH3 cells treated with (f) the vehicle and (g) OCT (10^{-6} M) for 72 h. Apoptotic and necrotic cells are compared with vehicle-treated cells in (f) and (g). A two-tailed unpaired Student's *t*-test is used for the statistical validation of B and C. *P < 0.05, **P < 0.01, and ****P < 0.0001.

environments. Specifically, the expression levels of SSTR2 and SSTR5, which are the predominant SSTR subtypes in GH-secreting adenoma [39], are significantly upregulated in GH3 cells cultured in 3D models (Fig. 2c). These results could facilitate the clinical management of GH-secreting tumors as SSTR2 and SSTR5 are the primary targets of somatostatin analogs used in the treatment of the corresponding medical condition [40]. Transmission electron microscopy (TEM) was used to evaluate the ultrastructure of 2D- and 3D-cultured GH3 cells. Fig. 2d and e shows representative TEM images that were used to compare the differences in cellular organization between the two models. Interestingly, 2D-cultured GH3 cells exhibited autophagic bodies and apoptosis, whereas those cultured in the proposed 3D model exhibited relatively intact intracellular structures. These observations indicate that the 3D culture system provides a more physiologically relevant environment for GH3 cells.

2.3. Improved somatostatin-analog responses of 3D-cultured GH3 cells

Subsequently, the effects of somatostatin analogs on the viability and GH secretion of GH3 cells were investigated. GH3 cells were treated with OCT (i.e., a somatostatin analog) in both 2D and 3D cell culture models. As shown in Fig. 3a and b, after six days of OCT exposure, a greater reduction in viability is observed in GH3 cells in HFMs than those in the control Petri dish; these findings are corroborated by statistical analyses (Fig. 3c and S6). Furthermore, the similar result was confirmed in comparison with GH3 cells in Matrigel (Fig. S7). Additionally, the PAS treatment caused a greater reduction in viability in GH3 cells in HFMs than those in the control Petri dish (Fig. S8).

GH concentrations in the culture media were evaluated to analyze the GH secretion of the GH3 cells. As shown in Fig. 3d and e, the GH levels in GH3 cells grown under 3D culture conditions were significantly greater than those grown under 2D culture conditions. Furthermore, the administration of OCT reduced the GH secretion of GH3 cells grown under 3D culture conditions to a greater extent than that of cells grown under 2D culture conditions. Additionally, TEM analysis indicates a greater increase in autophagic bodies, apoptotic cells, and necrotic cells in OCT-treated GH3 cells grown under 3D culture conditions compared to vehicle-treated GH3 cells grown under similar conditions (Fig. 3f and g).

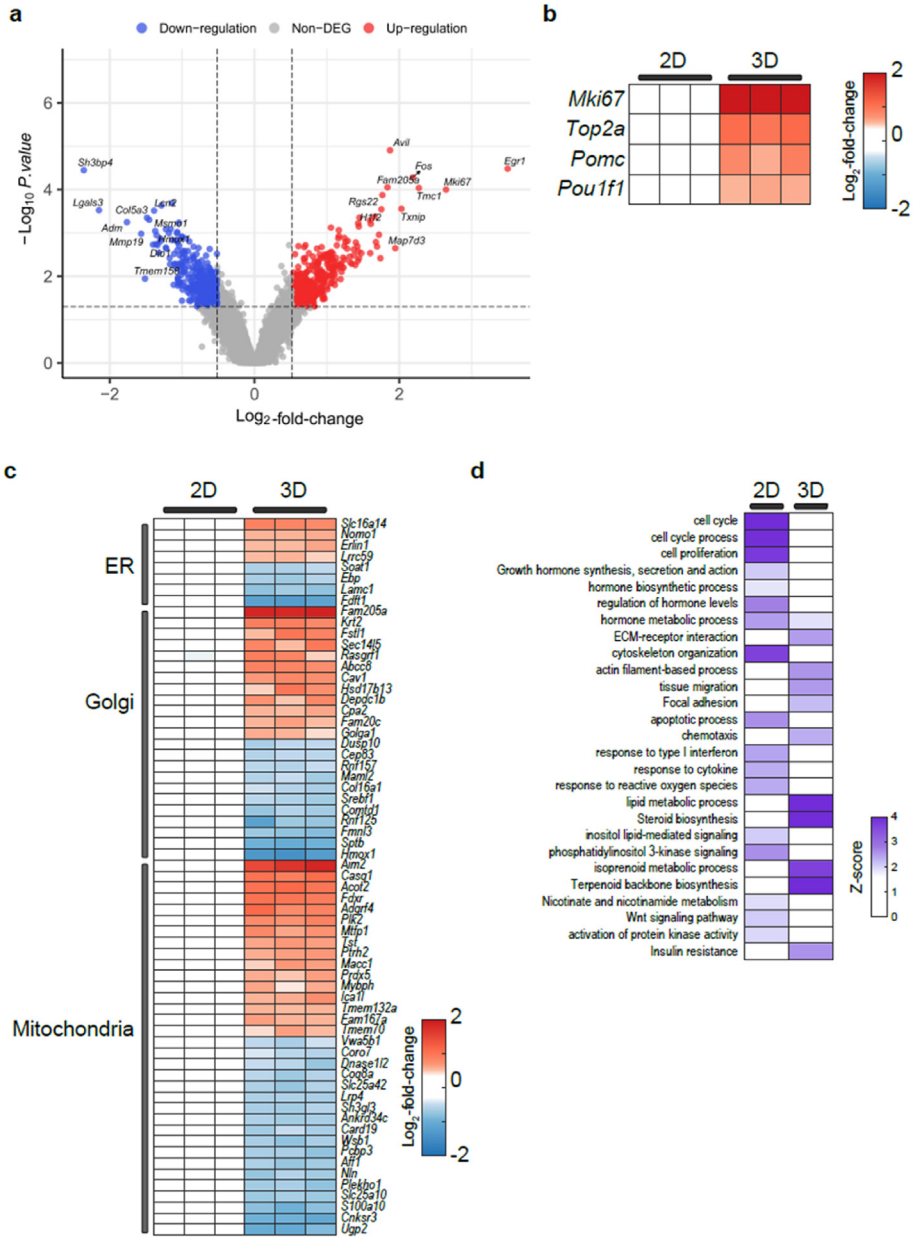

Fig. 4. Analysis of differentially expressed genes in GH3 cells cultured in 2D and 3D using bulk RNA sequencing data.
(a) A volcano plot showing the differentially expressed genes in the 2D and 3D cell cultures. The threshold of the y-axis is the cutoff of the overall P value (0.05), while that of the x-axis is the cutoff of the log2 fold change (±0.5) (b) A heatmap showing the critical genes for pituitary adenoma development in GH3 cells grown in the 3D and 2D cultures. Color bars indicate the gradients of the log2 fold change. (c) A heatmap showing the DEGs related endoplasmic reticulum (ER), Golgi apparatus (Golgi), and mitochondria. Color bars indicate the gradients of the log2 fold change. (d) A heatmap showing the functional enrichment analysis of 2D- and 3D-cultured GH3 cells. Color bars indicate the Z-score gradients.

2.4. Transcriptomic analysis of 2D and 3D in-vitro pituitary adenoma models

An RNA-seq analysis was used to gain the insight into the effects of growth dimensions on GH3 cells at the transcriptome level. A comparative analysis of RNA-seq data generated from the 3D and 2D culture models indicated a significant transcriptional response associated with the 3D culture environment. As shown in Fig. 4a, a significant upregulation of 424 genes and concomitant downregulation of 415 genes resulted in 839 differentially expressed genes (DEGs) which were observed in the 3D culture system. Notably, critical genes associated with pituitary adenoma development including the markers of proliferation, i.e., Ki-67 (*Mki67*), DNA topoisomerase II alpha (*Top2a*), proopiomelanocortin (*Pomc*), and POU class 1 homeobox 1 (*Pou1f1*) genes [41–43] were more significantly upregulated in the 3D culture model than in the 2D culture model (Fig. 4b).

DEG analysis also indicates a differential expression of gene sets related to the function of cellular organelles such as endoplasmic reticulum (ER), Golgi apparatus (Golgi), and mitochondria (Fig. 4c). Notably, the most highly upregulated genes including solute carrier family 16 member 14 (*Slc16a14*) [44] in the ER, family with sequence similarity 205 member A (*Fam205a*) [45] in the Golgi, and absent in melanoma 2 (*Aim2*) [46] in the mitochondria, significantly influenced tumor development and metabolism. Fig. 4d shows the DEG pathway analysis, which indicates a significant enrichment of several metabolic processes in the pituitary gland. Notably, as expected, a relatively greater positive enrichment of pathways related to GH secretion (including "GH synthesis, secretion and action" and "hormone biosynthetic process") was observed in the 3D culture model compared to the 2D culture model. Conversely, the pathways related to the sterol/cholesterol metabolism such as sterol biosynthetic, cholesterol biosynthetic, and cholesterol metabolic processes, were negatively enriched in the 3D culture model. Furthermore, DEGs associated with cell adhesion and cytoskeleton organization exhibited upregulation in the 3D culture model when compared to the 2D culture model. These observations indicate that the 3D culture environment significantly influenced the metabolic processes underlying GH secretion and sterol/cholesterol metabolism in the pituitary gland.

3. Discussion

In this study, highly porous HFM-based scaffolds were developed for 3D cell cultures and used to construct a 3D *in-vitro* cell-culture model for pituitary adenoma research. Highly-porous fibrillar hydrogel structures enable attachment/migration/development of various types of cells such as NIH3T3, PC12, SH-SY5Y, and even primarily cultured neurons [27] and facilitate nutrient exchange [47] (see also Fig. S9). A comparison of molecular characteristics of GH3 growth patterns under 2D- and 3D-culture conditions confirmed that GH3 cells seeded onto highly-porous HFM scaffolds showed more dispersed growth and higher depth profiles than those grown on flat Petri dishes. When 3D GH3 cell cultures were compared, cells tend to aggregate into spherical clusters due to the spatial constraint, whereas, the majority of cells are spatially distributed due to large voids created by leaching CA microbeads. Moreover, the typical Young's moduli of self-assembled fibrils of collagen type 1 range from several MPa to GPa, which is much higher than reconstructed matrices based on collagen which exhibits Young's moduli below kPa ranges, thus, mimic the soft tissue environment [48]. Although Young's modulus of an individual fiber in HFM (~700 kPa, Fig. S10) is higher than those of typical soft tissues such as brain, the collective behavior of fibers in HFM may result in actually lower stiffness, which is suitable for emulating soft tissues such as pituitary adenoma. Furthermore, the fabricated HFMs showed mechanical flexibility and permitted 3D microscopy imaging (e.g., laser scanning confocal microscopy) owing to their high optical transparency and minimal refraction/scattering. In addition to enhanced GH3 cell adhesion and viability, the gene expressions of SSTR2 and SSTR5 were significantly upregulated in GH3 cells cultured in the 3D model based on highly-porous HFMs; this may facilitate the clinical management of GH-secreting tumors [49,50].

TEM analysis indicates that GH3 cells cultured in the HFM-based 3D model comprised intact intracellular structures, whereas those cultured in the conventional 2D environment contained autophagic and apoptotic bodies. This indicates that a 3D culture system based on highly-porous HFMs may provide a more physiologically relevant environment for GH3 cell growth and function than a 2D culture system based on Petri dishes. The poor SSTR gene expression and the damaged status of GH3 cells in 2D-culture systems significantly limit the applicability of such systems in pituitary adenoma research [51]. The results of functional assays confirmed the greater applicability of the 3D culture system in pituitary adenoma research. GH3 cells in the HFM-based 3D-culture model showed improved somatostatin-analog responses (i.e., decreased cell viability and suppressed GH secretion) compared to those in the 2D culture model. Moreover, in bulk RNA-seq analysis (which was used to assess the transcriptomic profiles of GH3 cells), 3D cultured GH3 cells showed the significant upregulation of genes related to pituitary adenoma and a positive enrichment of pathways related to GH secretion, indicating the high potential applicability of GH3 cells cultured on highly porous HFMs as drug-screening platforms for pituitary-tumor treatment.

However, this study is associated with several limitations. First, a single cell line (GH3) derived from the pituitary adenoma of a female rat was used, which may not be representative of GH-secreting human pituitary adenomas [7]. Thus, further studies are required to develop *in-vitro* 3D cell culture models based on human pituitary tumor cells or induced pluripotent stem cells [52]. Additionally, this study examined the effects of only two somatostatin analogs (OCT and PAS) on GH secretion. The effects of other somatostatin analogs and acromegaly-therapy drugs [53] on the cell viability and GH secretion of the proposed 3D cell culture model should also be investigated.

4. Conclusions

In summary, a 3D *in-vitro* cell culture model for pituitary adenoma research was developed using HFMs and GH3 cells. GH3 cells grown in the proposed 3D model exhibited the increased cell dispersion and the up-regulation of specific somatostatin-receptor subtypes compared to those grown in traditional 2D cultures with high sensitivity to somatostatin analogs as indicated by functional assays and tumor-like profiles as indicated by transcriptome analysis. Therefore, the proposed 3D model provides a relatively more accurate representation of the physiological response to therapeutic agents of pituitary adenoma than traditional 2D cell culture models. The results of this study indicate that the newly developed 3D cell culture system may be utilized as an effective *in-vitro* model for studying GH-secreting tumors, facilitating the development of effective therapeutics for acromegaly and other related diseases.

5. Experimental section

5.1. Materials for fabricating HFMs

Partially hydrolyzed PVA with a hydrolysis degree of 87–89% and a molecular weight (MW) in the range of 85,000–124,000, a PAA solution (35 wt%) with an average MW of 100,000, CA with an average MW of 30,000, and PDL hydrobromide with a MW in the range of 70,000–150,000 were purchased from Sigma Aldrich Korea. Concentrated H_2SO_4 and N, N-dimethylformamide (DMF; 99.5% pure) were purchased from Duksan Chemical, Korea. Phosphate-buffered saline (1X) (PBS) was purchased from Thermo Fisher Scientific (Waltham, MA, USA). EP-grade acetone with a purity of 99.5% was purchased from OCI Chemicals (Korea). All the chemicals were used without further purification.

5.2. Fabrication of porous HFMs

To fabricate porous HFMs for a 3D cell culture scaffold, a PVA/PAA blend was electrospuned (to form nanofibers) and electrosprayed with a CA solution (to form sacrificial microbeads). To prepare the electrospun solution (comprising 12 wt% of PVA and 3 wt% of PAA), PVA powder was dissolved in distilled water at 90 °C, followed by the addition of a PAA solution. CA powder (1.7 g) was dissolved in a mixture of DMF and acetone (8.3 g; 3:2 vol ratio) and used as the electrospraying solution (containing 17 wt% of CA), as described in a previous publication [54]. A commercial electrospinning setup with a drum-type collector (ESR200RD, NanoNC) was used for simultaneous electrospinning and electrospraying; a 23 G blunt metal nozzle was used as the syringe. A constant flow rate of 0.4 mL/h was used, with a voltage of 20 kV and tip-to-collector distance of 13 cm. For crosslinking, the NFM with CA microbeads was annealed at 120 °C for 4 h. Subsequently, the mesh was sliced using a round-metal punch with a diameter of 28 mm and soaked in excess concentrated H_2SO_4 for 15 min (for hydrogelification and complete CA-microbead leaching) to increase its porosity. The mesh was then rinsed with distilled water for H_2SO_4 removal and CA degradation. The porous HFM formed was immersed in PBS, and its morphology was analyzed by laser scanning confocal microscopy with methylene blue staining.

5.3. Analysis of the HFM porosity

Z-stack images of the NFM with CA microbeads (before H_2SO_4 treatment) and porous HFM (after H_2SO_4 treatment) were recorded by laser scanning confocal microscopy after methylene blue staining (0.1 mg/mL). An excitation wavelength of 635 nm and an emission channel of 650–750 nm were used. Porosity was considered to be the void between the fibers, and the void fraction was calculated from Z-stack images using the ImageJ software. The ImageJ macro code for porosity analysis is provided in the Supporting Information. To confirm that CA-microbead leaching from the NFM increased its porosity, three types of HFM were fabricated. The compositions of these HFMs and the precursor solutions used for electrospinning and electrospraying are summarized in Table S1.

5.4. Cell cultures and drug preparation

GH3, a female-rat pituitary tumor cell line, was procured from a Korean cell line repository and maintained in Ham's F-12 medium (WELGENE, #LM 010-03), supplemented with 15% (v/v) of horse serum (Thermo Scientific, # 6050122), 2.5% (v/v) of fetal bovine serum (Gibco, #12483020), and 1% (v/v) of penicillin/streptomycin (WELGENE, #LS202-02) at 37 °C under CO_2 (5%). For 3D cell culture, the synthesized hydrogel fibers were washed with PBS (thrice) and subjected to UV-light irradiation for a minimum of 15 min before cell seeding. The GH3 cells were then dispersed onto the HFM. We added a small amount of culture medium, enough to cover the fibers. The cells were incubated at 37 °C for 1 h to allow for initial cell adhesion and facilitate attachment. To support subsequent cell growth and maintenance, fresh culture medium was added to each well (2 ml in single well of 6 well plate). All experiments were carried out with a cell confluence in the range of 75–80%. For subculturing, the cells were detached using 0.25% of trypsin-EDTA (Hyclone, #SH30042.02) for a maximum of 10 min.

OCT acetate and PAS were purchased from Novartis Pharmaceuticals for scientific investigation and diluted with 0.9% saline to specific concentrations. A live/dead assay with calcein AM (Invitrogen, #C1430) and ethidium homodimer-1 (Invitrogen, #E1169) was used to assess cell viability.

5.5. Cell viability assay

A total of 3.5×10^5 GH3 cells were seeded into hydrogel fibers (for 3D cell culture) and PDL-coated confocal dishes with a surface area of 3.5 cm^2 (for 2D cell culture), according to the manufacturer's protocol. After 24 h, the wells were individually treated with the vehicle (0.9% saline) or different concentrations of OCT (10^{-5}, 10^{-6}, or 10^{-7} M) for six days. Every 72 h, the medium containing OCT was replaced with a fresh medium. After six days, the cells were washed with Hanks' Balanced Salt Solution (HBSS, Gibco, #14025-092) and incubated with calcein AM and ethidium homodimer-1 (1:500 diluted solutions in HBSS) for 15 min at 37 °C under CO_2 (5%). Subsequently, the dye solution was removed, and the cells were washed with HBSS. The cells were then fixed in 4% glutaraldehyde (Sigma-Aldrich, #340855) in HBSS for 15 min at room temperature, before being examined by an upright confocal microscope (BX61WI body, FV1000 model system, Olympus Co. Ltd. Tokyo, Japan) at 20x with the excitation and emission wavelengths of calcein AM (494 and 517 nm, respectively) and ethidium homodimer-1 (528 and 617 nm, respectively). Images were recorded in the region of interest (ROI, 350 × 350) using the ImageJ software.

5.6. Immunofluorescence staining

Immunofluorescence with Alexa Fluor™ 546 phalloidin (F-actin, Invitrogen, #A22283), following the manufacturer's protocol, was used to investigate the cell morphology. A total of 3.5×10^7 GH3 cells were seeded onto hydrogel fibers (for 3D cell culture) and confocal dishes with a surface area of 3.5 cm^2 (for 2D cell culture). After a day, the cells were fixed with 4% paraformaldehyde (#HP2031, Biosesang, Seongnam, Korea) and permeabilized in 0.1% Triton X-100 in PBS for 15 min at room temperature. Subsequently, the cells were blocked with 1% of BSA and 1% of gelatin for 30 min, incubated in a 40x phalloidin blocking solution for 1 h, and examined using an upright confocal microscope (BX61WI body, FV1000 model system, Olympus Co. Ltd. Tokyo, Japan) at 20x with an excitation wavelength of 556 nm and emission wavelength of 570 nm.

5.7. TEM and SEM analysis

The specimens were first fixed for 12 h in a solution containing 2% glutaraldehyde and 2% paraformaldehyde in PBS (0.1 M) with a pH of 7.4. They were then washed with PBS (0.1 M) and post-fixed with 1% of OsO_4 in PBS (0.1 M) for 2 h. Subsequently, the specimens were dehydrated with an ascending series of ethanol concentrations (50%, 60%, 70%, 80%, 90%, 95%, 100%, and 100%) for 10 min each and infiltrated with propylene oxide for 10 min. They were then embedded using a Poly/Bed 812 kit (Polysciences, USA) and polymerized in an electron-microscope oven (TD-700, DOSAKA, Japan) at 65 °C for 12 h. Next, the specimen block was cut into 200-nm sections using a diamond knife on an ultramicrotome; the region of interest was cut into 80-nm-thin sections using an ultramicrotome. These sections were placed on copper grids, double-stained with 3% of uranyl acetate for 30 min and 3% of lead citrate for 7 min, and analyzed by a TEM instrument (JEM-1011; JEOL, Tokyo, Japan) equipped with a MegaView III CCD camera (Soft Imaging Systems, Germany) at an acceleration voltage of 80 kV. SEM and field emission (FE)-SEM (Jeol, JSM-7500F) images, recorded at 15 keV with Pt coatings for 180 s, were also analyzed.

5.8. ELISA assay

A total of 0.35×10^6 GH3 cells were seeded onto hydrogel fibers (for 3D cell culture) and 12 PDL-coated well plates (for 2D cell culture). After 24 h, the medium was replaced with a serum-free medium for 3 h to evaluate the GH baseline. Media with the vehicle or OCT (10^{-5}, 10^{-6}, or 10^{-7} M) in serum-free media were collected at the baseline, after 24 h, and after 48 h. The collecting medium was frozen (at −80 °C) immediately before analysis. The concentration of GH in the supernatant was determined using a rat Growth Hormone ELISA kit (Merck Millipore, #EZRMGH-45K), according to the manufacturer's instructions.

5.9. Quantitative reverse transcriptase-PCR (qRT-PCR) analysis

GH3 cells were harvested using 0.25% trypsin-ethylenediaminetetraacetic acid and washed thrice with PBS. The total RNA was extracted using a Total RNA extraction kit (Clear-STM, In Virus Tech, #IVT3001) according to the manufacturer's protocol. Subsequently, the total RNA (1 μg) was reverse-transcribed using a high-capacity cDNA Reverse Transcription kit (Applied Biosystems, Waltham, MA, USA; Thermo Fisher Scientific). To analyze gene expression, the CFX384 Touch Real-Time PCR detection system (Bio-Rad) and AmfiSure qGreen Q-PCR master mix (#Q5602; GenDEPOT, Katy, TX, USA) were used for qRT-PCR. The primer sequences are provided in Table S2.

5.10. RNA sequencing

The RNA quality in GH3 cells was assessed using an Agilent 2100 bioanalyzer. RNA sequencing data were analyzed and visualized using R (version 4.1.0); STAR (version 2.7.9) was used for trimming and alignment in the preprocessing pipeline. Kallisto (version 0.45.0) was used to automatically quantify transcript amounts from RNA FASTQ files. The DESeq2 package (version 1.32.0) was used for differential gene expression analysis; volcano plots were used to compare results without any interaction terms. The clusterProfiler package (version 4.0.5), as well as the Gene Ontology (GO) and Kyoto Encyclopedia of Genes and Genomes (KEGG) databases were used for pathway enrichment analysis. The pathway-analysis input list comprised significant values with an adjusted P-value of 0.05 or lower from the DEseq2 results. Input data were labeled using the Entrez ID; non-available gene names were automatically removed.

5.11. Statistical analysis

GraphPad Prism 9.0.0 (GraphPad Software Inc. San Diego, CA, USA) was used for all statistical analyses. Differences between groups were evaluated for statistical significance using the Student's *t*-test or one-way analysis of variance (ANOVA) followed by Tukey's post hoc test and Sidak's multiple comparison test. A statistical significance of $P < 0.05$ was used.

Funding

This research was supported by the Basic Science Research Program through the National Research Foundation of Korea funded by the Ministry of Education (2020R1C1C1004999, 2018-M3A7B407098, 2021R1A4A1022920), GIST Research Institute IIBR grants funded by the GIST in 2023, and the KHIDI-AZ Diabetes Research Program, and "Team Science Award" of Yonsei University College of Medicine (6-2022-0150).

Data and materials availability

Sequencing data were obtained from the Gene Expression Omnibus database (BioProject ID: PRNJA862187).

CRediT authorship contribution statement

Wooju Jeong: Methodology, Investigation, Software, Visualization, Writing – original draft. **Sungrok Wang:** Methodology, Investigation, Software, Visualization, Writing – original draft. **Yumin Kim:** Methodology, Formal analysis, Visualization. **Soohyun Lee:** Methodology. **Minhu Huang:** Methodology. **Jaeil Park:** Methodology. **Myung-Han Yoon:** Supervision, Conceptualization, Writing – review & editing. **Chang-Myung Oh:** Supervision, Conceptualization, Writing – original draft, Writing – review & editing. **Cheol Ryong Ku:** Supervision, Writing – review & editing.

Declaration of competing interest

The authors declare that they have no known competing financial interests or personal relationships that could have appeared to influence the work reported in this paper.

Appendix A. Supplementary data

Supplementary data to this article can be found online at https://doi.org/10.1016/j.smaim.2024.03.004.

References

[1] A. Colao, L.F.S. Grasso, A. Giustina, S. Melmed, P. Chanson, A.M. Pereira, R. Pivonello, Acromegaly, Nat. Rev. Dis. Prim. 5 (2019) 20, https://doi.org/10.1038/s41572-019-0071-6.
[2] M. Rolla, A. Jawiarczyk-Przybyłowska, J. Halupczok-Żyła, M. Kałużny, B.M. Konopka, I. Błoniecka, G. Zieliński, M. Bolanowski, Complications and Comorbidities of acromegaly—Retrospective study in polish center, Front. Endocrinol. 12 (2021) 642131, https://doi.org/10.3389/fendo.2021.642131.
[3] A. Colao, D. Ferone, P. Marzullo, G. Lombardi, Systemic complications of acromegaly: epidemiology, pathogenesis, and management, Endocr. Rev. 25 (2004) 102–152, https://doi.org/10.1210/er.2002-0022.
[4] J. McCabe, J. Ayuk, M. Sherlock, Treatment factors that influence mortality in acromegaly, Neuroendocrinology 103 (2016) 66–74, https://doi.org/10.1159/000375163.
[5] E.C. Coopmans, A.J. Van Der Lely, S.J.C.M.M. Neggers, Approach to the patient with treatment-resistant acromegaly, J. Clin. Endocrinol. Metabol. 107 (2022) 1759–1766, https://doi.org/10.1210/clinem/dgac037.
[6] A.H. Tashjian, Y. Yasumura, L. Levine, G.H. Sato, M.L. Parker, Establishment of clonal strains of rat pituitary tumor cells that secrete growth hormone [1, 2], Endocrinology 82 (1968) 342–352, https://doi.org/10.1210/endo-82-2-342.
[7] A. Dicitore, D. Saronni, G. Gaudenzi, S. Carra, M.C. Cantone, M.O. Borghi, L. Persani, G. Vitale, Long-term effects of somatostatin analogues in rat GH-secreting pituitary tumor cell lines, J. Endocrinol. Invest. 45 (2022) 29–41, https://doi.org/10.1007/s40618-021-01609-1.
[8] A.D. Van Den Brand, E. Rubinstein, M. Van Den Berg, M.B.M. Van Duursen, GH3 and RC-4BC cell lines are not suitable as in vitro models to study prolactin modulation and AHR responsiveness in rat pituitary, Mol. Cell. Endocrinol. 496 (2019) 110520, https://doi.org/10.1016/j.mce.2019.110520.
[9] X. Qian, L. Jin, J.P. Grande, R.V. Lloyd, Transforming growth factor-beta and p27 expression in pituitary cells, Endocrinology 137 (1996) 3051–3060, https://doi.org/10.1210/endo.137.7.8770931.
[10] J. Kovalevich, D. Langford, Considerations for the use of SH-SY5Y neuroblastoma cells in neurobiology, in: S. Amini, M.K. White (Eds.), Neuronal Cell Culture, Humana Press, Totowa, NJ, 2013, pp. 9–21, https://doi.org/10.1007/978-1-62703-640-5_2.
[11] K.A. Elias, R.I. Weiner, S.H. Mellon, Effect of extracellular matrix on prolactin secretion and mRNA accumulation in GH $_3$ cells, DNA Cell Biol. 9 (1990) 369–375, https://doi.org/10.1089/dna.1990.9.369.
[12] D. Antoni, H. Burckel, E. Josset, G. Noel, Three-dimensional cell culture: a breakthrough in vivo, IJMS 16 (2015) 5517–5527, https://doi.org/10.3390/ijms16035517.
[13] S.A. Langhans, Three-dimensional in vitro cell culture models in drug discovery and drug repositioning, Front. Pharmacol. 9 (2018) 6, https://doi.org/10.3389/fphar.2018.00006.
[14] A.M.K. Law, L. Rodriguez De La Fuente, T.J. Grundy, G. Fang, F. Valdes-Mora, D. Gallego-Ortega, Advancements in 3D cell culture systems for personalizing anti-cancer therapies, Front. Oncol. 11 (2021) 782766, https://doi.org/10.3389/fonc.2021.782766.
[15] C. Jensen, Y. Teng, Is it time to start transitioning from 2D to 3D cell culture? Front. Mol. Biosci. 7 (2020) 33, https://doi.org/10.3389/fmolb.2020.00033.
[16] D. Baruffaldi, G. Palmara, C. Pirri, F. Frascella, 3D cell culture: recent development in materials with tunable stiffness, ACS Appl. Bio Mater. 4 (2021) 2233–2250, https://doi.org/10.1021/acsabm.0c01472.
[17] Y. Ma, X. Zhang, S. Tang, L. Xue, J. Wang, X. Zhang, Extended preconditioning on soft matrices directs human mesenchymal stem cell fate via YAP transcriptional activity and chromatin organization, APL Bioeng. 7 (2023) 016110, https://doi.org/10.1063/5.0124424.
[18] Y. Ma, T. Han, Q. Yang, J. Wang, B. Feng, Y. Jia, Z. Wei, F. Xu, Viscoelastic cell microenvironment: hydrogel-based strategy for recapitulating dynamic ECM mechanics, Adv. Funct. Mater. 31 (2021) 2100848, https://doi.org/10.1002/adfm.202100848.
[19] N. Shi, J. Wang, S. Tang, H. Zhang, Z. Wei, A. Li, Y. Ma, F. Xu, Matrix nonlinear viscoelasticity regulates skeletal myogenesis through MRTF nuclear localization and nuclear mechanotransduction, Small (2023) 2305218, https://doi.org/10.1002/smll.202305218.
[20] N. Shi, Y. Li, L. Chang, G. Zhao, G. Jin, Y. Lyu, G.M. Genin, Y. Ma, F. Xu, A 3D, magnetically actuated, aligned collagen fiber hydrogel platform recapitulates physical microenvironment of myoblasts for enhancing myogenesis, Small Methods 5 (2021) 2100276, https://doi.org/10.1002/smtd.202100276.

[21] D. Zhang, W. Hugo, P. Redublo, H. Miao, M. Bergsneider, M.B. Wang, W. Kim, W.H. Yong, A.P. Heaney, A human ACTH-secreting corticotroph tumoroid model, EBioMedicine 66 (2021) 103294, https://doi.org/10.1016/j.ebiom.2021.103294.
[22] L. Krokker, B. Szabó, K. Németh, R. Tóháti, B. Sarkadi, K. Mészáros, A. Patócs, H. Butz, Three dimensional cell culturing for modeling adrenal and pituitary tumors, Pathol. Oncol. Res. 27 (2021) 640676, https://doi.org/10.3389/pore.2021.640676.
[23] Y.-J. Jeng, M.Y. Kochukov, C.S. Watson, Membrane estrogen receptor-α-mediated nongenomic actions of phytoestrogens in $GH_3/B_6/F_{10}$ pituitary tumor cells, JMS 4 (2009) 2, https://doi.org/10.1186/1750-2187-4-2.
[24] K. Fujiwara, D. Jindatip, M. Kikuchi, T. Yashiro, In situ hybridization reveals that type I and III collagens are produced by pericytes in the anterior pituitary gland of rats, Cell Tissue Res. 342 (2010) 491–495, https://doi.org/10.1007/s00441-010-1078-1.
[25] P. Li, D. Zhang, S. Ma, P. Kang, C. Zhang, B. Mao, W. Zhou, X. Wang, J. Peng, L. Yuan, Y. Wang, J. Diao, W. Jia, Consistency of pituitary adenomas: amounts of collagen types I and III and the predictive value of T2WI MRI, Exp. Ther. Med. 22 (2021) 1255, https://doi.org/10.3892/etm.2021.10690.
[26] T. Iskratsch, H. Wolfenson, M.P. Sheetz, Appreciating force and shape — the rise of mechanotransduction in cell biology, Nat. Rev. Mol. Cell Biol. 15 (2014) 825–833, https://doi.org/10.1038/nrm3903.
[27] W.Y. Wang, C.D. Davidson, D. Lin, B.M. Baker, Actomyosin contractility-dependent matrix stretch and recoil induces rapid cell migration, Nat. Commun. 10 (2019) 1186, https://doi.org/10.1038/s41467-019-09121-0.
[28] B.M. Baker, B. Trappmann, W.Y. Wang, M.S. Sakar, I.L. Kim, V.B. Shenoy, J.A. Burdick, C.S. Chen, Cell-mediated fibre recruitment drives extracellular matrix mechanosensing in engineered fibrillar microenvironments, Nat. Mater. 14 (2015) 1262–1268, https://doi.org/10.1038/nmat4444.
[29] J. Wu, Y. Hong, Enhancing cell infiltration of electrospun fibrous scaffolds in tissue regeneration, Bioact. Mater. 1 (2016) 56–64, https://doi.org/10.1016/j.bioactmat.2016.07.001.
[30] B.L.-P. Lee, H. Jeon, A. Wang, Z. Yan, J. Yu, C. Grigoropoulos, S. Li, Femtosecond laser ablation enhances cell infiltration into three-dimensional electrospun scaffolds, Acta Biomater. 8 (2012) 2648–2658, https://doi.org/10.1016/j.actbio.2012.04.023.
[31] M.K. Joshi, H.R. Pant, A.P. Tiwari, H.J. Kim, C.H. Park, C.S. Kim, Multi-layered macroporous three-dimensional nanofibrous scaffold via a novel gas foaming technique, Chem. Eng. J. 275 (2015) 79–88, https://doi.org/10.1016/j.cej.2015.03.121.
[32] A.A. Bulysheva, G.L. Bowlin, S.P. Petrova, W.A. Yeudall, Enhanced chemoresistance of squamous carcinoma cells grown in 3D cryogenic electrospun scaffolds, Biomed. Mater. 8 (2013) 055009, https://doi.org/10.1088/1748-6041/8/5/055009.
[33] M.F. Leong, W.Y. Chan, K.S. Chian, M.Z. Rasheed, J.M. Anderson, Fabrication and *in vitro* and *in vivo* cell infiltration study of a bilayered cryogenic electrospun poly(D,L-lactide) scaffold, J. Biomed. Mater. Res. 9999A (2010), https://doi.org/10.1002/jbm.a.32795. NA-NA.
[34] M. Simonet, O.D. Schneider, P. Neuenschwander, W.J. Stark, Ultraporous 3D polymer meshes by low-temperature electrospinning: use of ice crystals as a removable void template, Polym. Eng. Sci. 47 (2007) 2020–2026, https://doi.org/10.1002/pen.20914.
[35] D.-H. Kang, D. Kim, S. Wang, D. Song, M.-H. Yoon, Water-insoluble, nanocrystalline, and hydrogel fibrillar scaffolds for biomedical applications, Polym. J. 50 (2018) 637–647, https://doi.org/10.1038/s41428-018-0053-7.
[36] J. Park, T.T.C. Nguyen, S.-J. Lee, S. Wang, D. Heo, D.-H. Kang, A. Tipan-Quishpe, W.-J. Lee, J. Lee, S.Y. Yang, M.-H. Yoon, Instant formation of horizontally ordered nanofibrous hydrogel films and direct investigation of peculiar neuronal cell behaviors atop, Biomater. Res. 27 (2023) 19, https://doi.org/10.1186/s40824-023-00344-3.
[37] D.-H. Kang, S. Wang, M. Goh, J. Park, H. Na, W.-J. Lee, Y. Kim, M.S. Rahman, G. Tae, M.-H. Yoon, Synthesis of superabsorbent hydrogels with predefined geometries and controlled swelling properties for versatile 3D cell culture scaffolds, ACS Appl. Mater. Interfaces 16 (2024) 3031–3041, https://doi.org/10.1021/acsami.3c11999.
[38] T. Sone, T. Yamazaki, S. Oya, Treatment of polyvinylalcohol with high concentrated sulfuric acid and the dyeing of treated polyvinylalcohol, Sen-i Gakkaishi 27 (1971) 406–409, https://doi.org/10.2115/fiber.27.406.
[39] N. Ionovici, M. Carsote, D.C. Terzea, A.M. Predescu, A.-M. Rauten, M. Popescu, Somatostatin receptors in normal and acromegalic somatotroph cells: the U-turn of the clinician to immunohistochemistry report – a review, Rom. J. Morphol. Embryol. 61 (2020) 353–359, https://doi.org/10.47162/RJME.61.2.05.
[40] M. Gomes-Porras, J. Cárdenas-Salas, C. Álvarez-Escolá, Somatostatin analogs in clinical practice: a review, IJMS 21 (2020) 1682, https://doi.org/10.3390/ijms21051682.
[41] H. Zhang, C. Xu, N. Sun, Y. Zhou, X. Yu, X. Yan, Q. Zhang, Gene expression profiling analysis of MENX-associated rat pituitary adenomas contributes to understand molecular mechanisms of human pituitary adenomas, Oncol. Lett. 11 (2016) 125–133, https://doi.org/10.3892/ol.2015.3904.
[42] V. Ghatnatti, B. Vastrad, S. Patil, C. Vastrad, I. Kottursheti, Department of endocrinology, J N medical College, belagavi and KLE academy of higher education & research 590010, Karnataka, India, department of biochemistry, basaveshwar College of pharmacy, gadag, Karnataka 582103, India, department of obstetrics and gynaecology, J N medical College, belagavi and KLE academy of higher education & research 590010, Karnataka, India, biostatistics and bioinformatics, chanabasava nilaya, bharthinagar, dharwad 580001, karanataka, India, department of ayurveda, rajiv gandhi education society's ayurvedic medical College, ron 562209, karanataka, India, identification of potential and novel target genes in pituitary prolactinoma by bioinformatics analysis, AIMS Neuroscience 8 (2021) 254–283, https://doi.org/10.3934/Neuroscience.2021014.
[43] W. Wang, Z. Xu, L. Fu, W. Liu, X. Li, Pathogenesis analysis of pituitary adenoma based on gene expression profiling, Oncol. Lett. 8 (2014) 2423–2430, https://doi.org/10.3892/ol.2014.2613.
[44] J. Li, J. Xie, D. Wu, L. Chen, Z. Gong, R. Wu, Y. Hu, J. Zhao, Y. Xu, A pan-cancer analysis revealed the role of the SLC16 family in cancer, Channels 15 (2021) 528–540, https://doi.org/10.1080/19336950.2021.1965422.
[45] M.A. Skowron, P. Petzsch, K. Hardt, N. Wagner, M. Beier, S. Stepanow, M. Drechsler, H. Rieder, K. Köhrer, G. Niegisch, M.J. Hoffmann, W.A. Schulz, Distinctive mutational spectrum and karyotype disruption in long-term cisplatin-treated urothelial carcinoma cell lines, Sci. Rep. 9 (2019) 14476, https://doi.org/10.1038/s41598-019-50891-w.
[46] Y. Qin, L. Pan, T. Qin, H. Ruan, Y. Zhang, Y. Zhang, J. Li, J. Yang, W. Li, Pan-cancer analysis of AIM2 inflammasomes with potential implications for immunotherapy in human cancer: a bulk omics research and single cell sequencing validation, Front. Immunol. 13 (2022) 998266, https://doi.org/10.3389/fimmu.2022.998266.
[47] G. Kim, W. Kim, Highly porous 3D nanofiber scaffold using an electrospinning technique, J. Biomed. Mater. Res. 81B (2007) 104–110, https://doi.org/10.1002/jbm.b.30642.
[48] A. Saraswathibhatla, D. Indana, O. Chaudhuri, Cell–extracellular matrix mechanotransduction in 3D, Nat. Rev. Mol. Cell Biol. 24 (2023) 495–516, https://doi.org/10.1038/s41580-023-00583-1.
[49] R. Pichler, O. Kalev, B. Tomancok, M. Sonnberger, D. Ehrlich, M. Hodolic, Somatostatin receptor subtype expression in patients with acromegaly and complicated clinical course, Diagnostics 11 (2021) 1050, https://doi.org/10.3390/diagnostics11061050.
[50] D. Iacovazzo, E. Carlsen, F. Lugli, S. Chiloiro, S. Piacentini, A. Bianchi, A. Giampietro, M. Mormando, A.J. Clear, F. Doglietto, C. Anile, G. Maira, L. Lauriola, G. Rindi, F. Roncaroli, A. Pontecorvi, M. Korbonits, L. De Marinis, Factors predicting pasireotide responsiveness in somatotroph pituitary adenomas resistant to first-generation somatostatin analogues: an immunohistochemical study, Eur. J. Endocrinol. 174 (2016) 241–250, https://doi.org/10.1530/EJE-15-0832.
[51] R. Saksis, O. Rogoza, H. Niedra, K. Megnis, I. Mandrika, I. Balcere, L. Steina, J. Stukens, A. Breiksa, J. Nazarovs, J. Sokolovska, I. Konrade, R. Peculis, V. Rovite, Transcriptome of GH-producing pituitary neuroendocrine tumours and models are significantly affected by somatostatin analogues, Cancer Cell Int. 23 (2023) 25, https://doi.org/10.1186/s12935-023-02863-4.
[52] B. Zimmer, J. Piao, K. Ramnarine, M.J. Tomishima, V. Tabar, L. Studer, Derivation of diverse hormone-releasing pituitary cells from human pluripotent stem cells, Stem Cell Rep. 6 (2016) 858–872, https://doi.org/10.1016/j.stemcr.2016.05.005.
[53] S.O. Chin, C.R. Ku, B.J. Kim, S.-W. Kim, K.H. Park, K.H. Song, S. Oh, H.K. Yoon, E.J. Lee, J.M. Lee, J.S. Lim, J.H. Kim, K.J. Kim, H.Y. Jin, D.J. Kim, K.A. Lee, S.-S. Moon, D.J. Lim, D.Y. Shin, S.H. Kim, M.J. Kwon, H.Y. Kim, J.H. Kim, D.S. Kim, C.H. Kim, Medical treatment with somatostatin analogues in acromegaly: position statement, Endocrinol Metab 34 (2019) 53, https://doi.org/10.3803/EnM.2019.34.1.53.
[54] H. Lee, M. Nishino, D. Sohn, J.S. Lee, I.S. Kim, Control of the morphology of cellulose acetate nanofibers via electrospinning, Cellulose 25 (2018) 2829–2837, https://doi.org/10.1007/s10570-018-1744-0.